










Article

Carbon Dioxide Optical Sensing using Tapered and Coated LPGs and Neural Networks

Manuella C. de Oliveira¹, Felipe O. Barino¹, Nelson A. Cevidanes¹, Thales A. Curty¹
Ulysses R. C. Vitor¹ Jose A. Garcia Souto² Pablo Acedo² Diogo Coelho¹ Alexandre B. dos Santos¹

¹Dept. of Electrical Circuits, Universidade Federal de Juiz de Fora, Juiz de Fora, Brazil,
manuella.oliveira@engenharia.ufjf.br, felipe.barino@engenharia.ufjf.br, ncevidanes@gmail.com,
thales.curty@engenharia.ufjf.br, ulysses.vitor@engenharia.ufjf.br, diogo.coelho@ufjf.br,
alexandre.bessa@ufjf.edu.br

²Dept. of Electronic Technology, Universidad Carlos III de Madrid, Madrid, Spain, jsouto@ing.uc3m.es,
pag@ing.uc3m.es

Abstract— This work presents the development of a refractive index sensing methodology for measuring carbon dioxide concentrations, considering the effect of temperature environment. We propose and demonstrate, using simulations, the use of tapered and coated Long Period Gratings as a way to enhance the refractive index sensitivity. In addition, artificial neural networks were used to improve the estimation of carbon dioxide concentration, considering the cross-sensitivity effect with temperature.

Index Terms— Artificial Neural Networks, Carbon Dioxide, LPG, Optical Fiber Sensors.

I. INTRODUCTION

Nowadays, the demand for low-cost sensors that indicate the presence or concentration of gases in real-time, such as carbon dioxide (CO₂), in industrial and clinical environments has acquired growing importance [1], [2].

Increased CO₂ concentrations in agricultural barns can indicate grain degradation in the food industry [3]. Furthermore, sudden and significant increases in gas levels could signal fugitive emissions events. Note that an abnormal increase in CO₂ might indicate that a reservoir containing such gas might be leaking. These events can pose risks to both worker health and the environment. They may also discontinue manufacturing, which would lead to financial issues.

In the clinical field, the amount of CO₂ gas exhaled by a patient is one of the parameters used to diagnose hypermetabolic conditions such as sepsis [3], which may offer the best opportunity for actions that may improve survival.

In such scenarios, the use of fiber optic sensing devices are indicated because they are compact, lightweight, immune to electromagnetic interference, and can be used in extreme conditions, allowing real-time remote monitoring without the need for electrical energy at the sensing point [3]. Among the different types of fiber optic sensors, long period gratings (LPGs) have been widely used for measuring the variation of the external refractive index (RI) [3]–[5]

LPGs are composed of a periodic modulation of the effective RI of the fiber core, ranging from tens to hundreds of micrometers [6]. In these devices, there is a coupling between the fundamental core mode (LP₀₁) and a series of m co-propagating cladding modes (LP_{0m}). As a result of this coupling, the

LPG transmission spectrum shows a series of attenuation (resonant wavelengths) peaks. This condition, called phase matching, is given as [6]–[8].

$$\lambda^m = (n_{eff,core}^{01} - n_{eff,cladding}^{0m}) \Lambda, \quad (1)$$

where λ^m is the resonant wavelength of the m^{th} -order cladding mode, $n_{eff,core}^{01}$ and $n_{eff,cladding}^{0m}$ are the effective RI of the fundamental core mode and the m^{th} -order cladding mode, respectively. Λ is the period of the grating.

Equation 1 shows the dependence between the resonant wavelength, the effective refractive indexes, and the period of the grating. Any changes in these parameters cause shifts in the resonant wavelength, allowing the use of LPGs in sensing applications such as temperature variations, mechanical deformations, and RI of the external environment [8].

Tapered fibers are made by stretching and heating the optical waveguide, which results in smaller fiber core and cladding diameters. As a result, the difference between the effective RI of the core mode and the cladding modes decreases. This causes the light to be less confined to the core and allows it to spread more into the cladding, increasing the interaction with the surrounding material. Indeed, the reduction in fiber's diameter means that the light has less material to be guided through. Consequently, there is a more pronounced evanescent wave, which improves the sensitivity to external influences such as temperature and RI variation [9]. Furthermore, the experimental and simulation results in [10] showed the sensitivity of tapered optical fiber gas sensors increases by decreasing the taper diameter. Indeed, the cross-sensitivity of temperature fluctuations and gas concentration complicates data analysis, especially in tapered sensors. These values, however, can be estimated by observing the variation of two or more resonance frequencies.

In this context, Artificial Neural Networks (ANNs) can be applied to fiber sensor data processing in several situations, whether for quantitative or qualitative analysis of some parameter [11], [12], to implement multi-parameter sensing [13], [14], or to resolve non-linearities in multi-parameter systems [15]. In nonlinear regression, the multilayer perceptron (MLP) stands out among ANNs because, with a basic topology, it can estimate any function with a finite number of discontinuities [16]. The literature provides a thorough description of how ANN is used as a spectrum processing technique in LPG-based optical sensors. Typically, spectral characteristics are taken and supplied into the neural network, after which the measurement is obtained [17]. In [18] and [19], two LPGs were used in conjunction with an MLP to measure temperature and bending curvature for the embedded long period grating bending sensors.

Additionally, the authors in [20] demonstrated the concept of a LPG-based CO₂ sensor that was covered in a metal organic framework material. However, the implementation of multi-parameter sensing analysis was not realized.

In this work, we created in Optigrating software a tapered and coated LPG to increase its sensitivity to external RI with the objective of sensing different CO₂ concentrations, using Optisystem simulations. The proposed method was based on the interrogation of two resonant wavelengths and allows continuous detection under the effect of cross-sensitivity due to the temperature in the sensor. Additionally, the spectral data are sent into a Python-created artificial neural network (ANN) to provide a qualitative analysis of the CO₂ concentration in the surrounding environment.

As far as we know, the use of coated and tapered LPG in combination with ANN methods for

cross-sensitivity between temperature variations and CO₂ concentration has not been addressed before.

II. METHODOLOGY

As previously stated, the LPG was created in Optigrating 4.2 software, been designed according to the commercial fiber with core and cladding diameters of approximately 8 μ m and 125 μ m. In order to approximate the resonant wavelengths to the 1.55 μ m region and improve the LPG response to wavelength and power variation, the fiber core and cladding diameters were tapered to 88% of the original value, which corresponds to 110 μ m for the cladding, 7.2 μ m for the core, and a grating period of 590 μ m. The optical spectrum of the tapered LPG created and used in our simulations is depicted in Fig. 1.

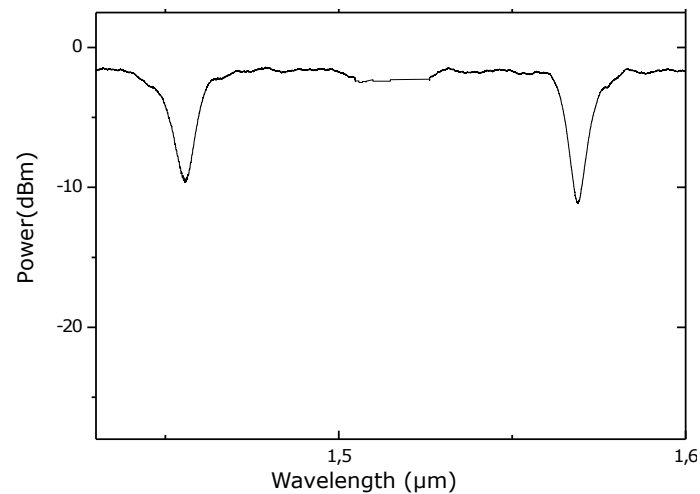


Fig. 1. LPG spectrum used in the measurements. As aforementioned, the spectrum is composed by two resonant wavelengths.

The interrogation process was simulated in Optisystem 7.0 and consists of an optical broadband source (BBS) and two Bragg gratings (FBGs), each one centered in the wavelength region of each of the two valleys of the LPG response, represented in Fig. 1, and with 1nm of bandwidth. The signals reflected by the FBGs are introduced into an optical spectrum analyzer (OSA) to evaluate these resonance wavelengths. The proposed sensing scheme is illustrated in Fig. 2.

In order to increase measurement efficiency for CO₂, Python-based ANN approaches were utilized to estimate the gas's concentration considering the impact of temperature variations in the surrounding area. The MLP used in this work has a single hidden layer with two inputs, 13 neurons in the hidden layer, and one output, being classified as a topology 2 \times 13 \times 1. The inputs are the distance between the resonant wavelengths and the attenuation differences between them. The hyperparameters were adjusted to identify the optimal topology using Bayesian search [21], which were the 13 neurons in the hidden layer. The output is the estimated concentration of CO₂ in the environment. Thus, the MLP outputs the temperature-compensated CO₂ concentration. In the further sections we show that the temperature effect adds non-linearities at the CO₂ concentration response. This effect was observed by the change in RI sensitivity due to the temperature change.

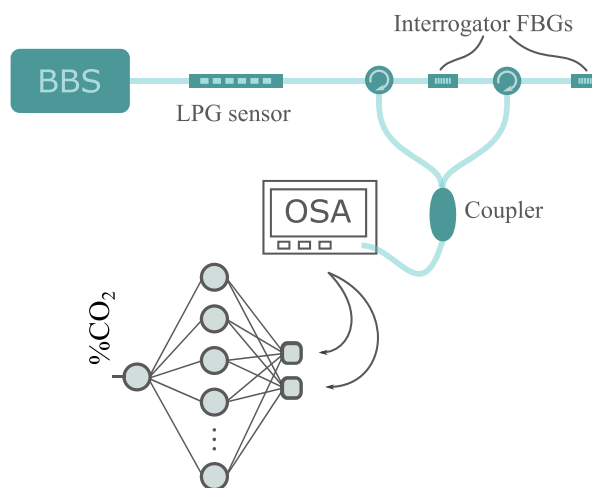


Fig. 2. Proposed sensing system. BBS is the broadband source.

III. MEASUREMENTS AND RESULTS

First, the spectral response of LPG was analyzed, considering variations in external RI and temperature individually. Then, we investigated the sensor response under the effects of RI change and temperature variations at the same time, therefore taking into account the cross-sensitivity effect.

The LPG was characterized in relation to the external RI of the medium, which may be correlated with CO₂ concentrations ranging from 0 to 50%. However, this gas has a very low refractive index, as discussed in [22]. Therefore, to identify the presence of the gas, it is necessary to cover the original sensor with a layer sensitive to CO₂, which will absorb the gas molecules resulting in higher values of the external RI compared to the cladding, as represented in Table I [22]. In the coating process, a dye-doped sol-gel layer is considered, as performed in [23]. The sol-gel, which is an organically modified silicate (ORMOSIL) layer, was doped with the dye Pyranine (C₁₆H₇Na₃O₁₀S₃) [23] [24]. After the sol-gel forms a porous glass matrix, the carbon dioxide dissolves in the moisture to generate carbonic acid, which then interacts only with the dye [23]. The LPG's resonant wavelengths shift as a result of the refractive index changes brought on by this reaction. The concentration of carbon dioxide in the gas directly affects these changes.

TABLE I. RELATIONSHIP BETWEEN RI OF THE LAYER SENSITIVE MATERIAL AND CO₂ CONCENTRATION [22].

CO ₂ (%) Concentration	Coating RI
0	1.3558
10	1.3567
20	1.3570
30	1.3571
40	1.3572
50	1.3573

Additionally, because of the dye CO₂ reaction temperature range, the effect of temperature cross-sensitivity was examined in the room temperature range of 22°C to 27°C [24]. Since each mode has a unique sensitivity to each parameter, the two resonant wavelengths alter differently and allow for cross-sensitivity compensation. Thus, the measurements of the two resonance wavelength variations and power levels were performed to estimate when the CO₂ concentration and temperature changed.

A. External RI Sensibility (CO_2 Concentration)

The influence of the RI sensitive layer of the 88% tapered LPG sensor was investigated, focusing on the characteristics of the two resonance wavelengths of the spectrum, as illustrated in Fig. 1. The characterization of the LPG resonance wavelengths variation was performed, considering a RI change from 1 to 1.4 and a constant temperature of 25°C, as can be seen in Fig. 3 for the second resonance wavelength. Considering the first resonance wavelength, a RI sensitivity equal to -7.56352nm/RIU was obtained, while for the second, it was -26.16287nm/RIU , considering a linear approximation at the 1.3558 1.3573 range.

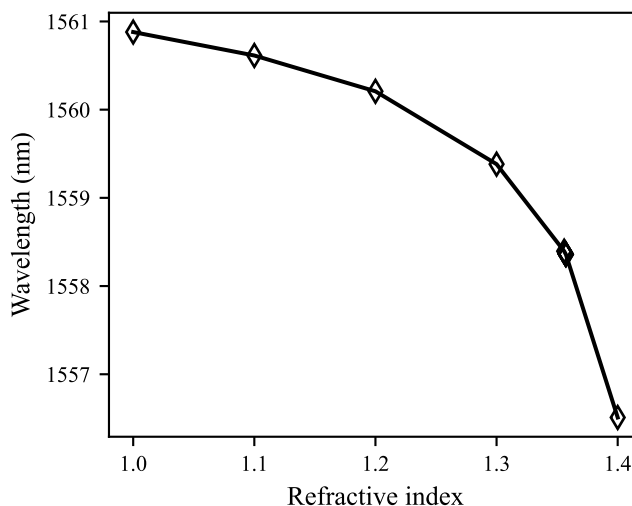


Fig. 3. Variation of the second resonance wavelength in relation to the refractive index.

Note that this sensitivity covers the LPG's full RI scale. The specific RI's range of interest, related to the coating layer's RI due to CO_2 concentration was studied in depth for several temperature values. The CO_2 concentration impact on the sensor at 23°C can be seen in Fig. 4 (a) and Fig. 4 (b), respectively. At this temperature, the CO_2 sensitivity was calculated as $1.22 \cdot 10^{-4} \text{ dB}/\%CO_2$ and $0.54 \text{ pm}/\%CO_2$,

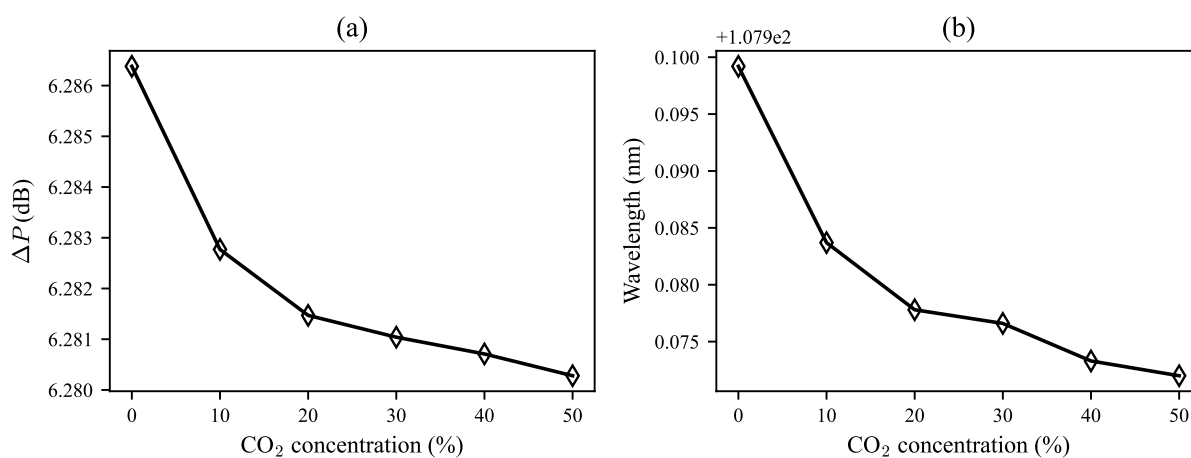


Fig. 4. Sensitivity to CO_2 concentration regarding (a) attenuation differences between the two resonance wavelengths and (b) second resonant wavelength.

regarding the dip attenuation difference (ΔP) and the second resonant wavelength.

B. Temperature sensitivity

In addition to the RI variations, changes were performed only in the temperature of the external environment, as proof that the temperature outside the fiber directly interferes with it and consequently with future RI measurements. As previously mentioned, the temperature variation range was 22°C to 27°C, and in this case, the external RI was kept constant so that this parameter did not interfere with the variation of the resonance wavelengths when the LPG was only sensitive to temperature. In Fig. 5 and 6 it is possible to verify the changes of the first and second resonance wavelengths, respectively, when alterations in temperature occur, keeping the RI constant. It is also verified the characteristic equations, which relate the variation of the wavelength (y) with the temperature (x), for each resonance wavelength.

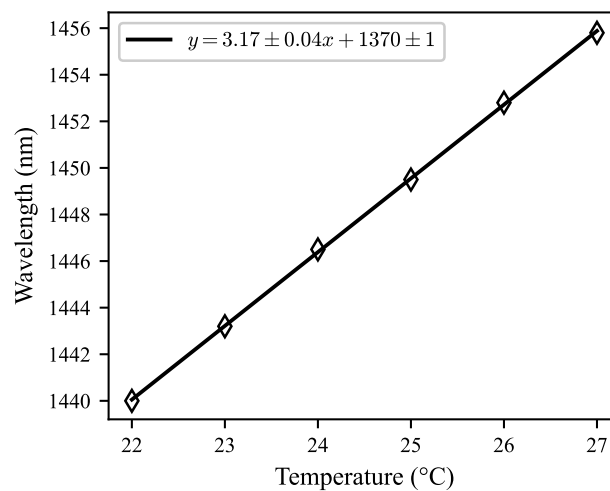


Fig. 5. First resonance wavelength variation in relation to temperature.

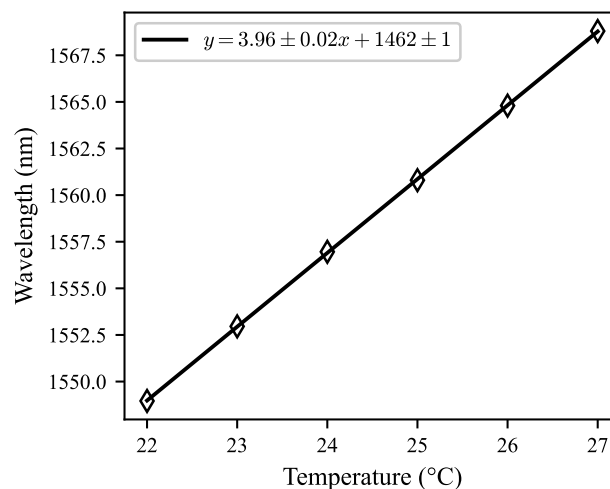


Fig. 6. Second resonance wavelength variation in relation to temperature.

C. Cross-sensitivity between Temperature Variations and Gas Concentration

To analyze CO₂ gas concentrations and temperature simultaneously, we propose a sensing method based on measuring the differences between LPG resonance wavelengths. First, variations in temperature (22°C - 27°C) and RI of the LPG were performed.

After that, the differences between the resonance wavelengths were measured, which allowed us to identify how the refractive index and temperature affect the sensor. The CO₂ concentration could be identified then by the relationship given in Table I. The equation (2) was obtained by measuring the differences between the two resonance wavelengths when the temperature is changed.

$$T = (1.295 \pm 0.001) \times \Delta\lambda - (116.85 \pm 0.09) \quad (2)$$

where T is the temperature in °C and $\Delta\lambda$ is the difference between wavelengths in nm.

Considering the different possible values of temperature, it is possible to measure the value of the external RI for different values of this parameter, with respect to the difference between the resonance wavelengths, as shown in Table II, where n is the desired external RI value.

Assume, for example, an environment where the measured difference between the resonance wavelengths is 109.05nm. Using Table II, it is possible to observe a temperature of 24.4°C. The value of n found was 1.357042, which represents (according to Table I) a concentration of approximately 20% of CO₂ in the environment.

We can see from Table II that the RI sensitivity changes depending on the temperature, thus introducing non-linearities for the CO₂ concentration measurement. Furthermore, we used an ANN to solve this dual-parameters cross-sensitivity issue, as ANNs are global approximators. Hence, the ANN allows the temperature compensations of the CO₂ concentration measurements.

TABLE II. TEMPERATURE AND RI WITH THE DIFFERENCE IN RESONANT WAVELENGTHS.

$\Delta\lambda$ (nm)	T (°C)	Characteristic Equation
107.21 – 107.24	22	$\Delta\lambda = -18.39088 n + 132.17673$
107.97 – 107.99	23	$\Delta\lambda = -18.13681 n + 132.58936$
108.73 – 108.77	24	$\Delta\lambda = -18.46254 n + 133.79597$
109.04 – 109.08	24.4	$\Delta\lambda = -18.54723 n + 134.21938$
109.27 – 109.31	24.7	$\Delta\lambda = -18.28339 n + 134.09296$
109.5 – 109.54	25	$\Delta\lambda = -18.5993 n + 134.7541$
109.74 – 109.78	25.3	$\Delta\lambda = -18.95114 n + 135.46455$
109.97 – 110.199	25.6	$\Delta\lambda = -20.20847 n + 137.40479$
110.2 – 110.24	25.9	$\Delta\lambda = -19.25407 n + 136.34364$
110.44 – 110.48	26.2	$\Delta\lambda = -18.87948 n + 136.07072$
110.68 – 110.71	26.5	$\Delta\lambda = -18.70033 n + 136.06325$
110.91 – 110.95	26.8	$\Delta\lambda = -19.25081 n + 137.04687$
111.07 – 111.11	27	$\Delta\lambda = -21.06515 n + 139.6685$

D. Estimation of CO₂ concentration using ANNs

To increase the accuracy of the CO₂ measurements, a neural network was utilized to estimate the concentration of this gas. The machine learning model was developed in Python, using the Keras framework running TensorFlow backend at room temperature. TensorFlow was employed because of its simple repeatability and high-level interface [25].

As aforementioned, the ANN has two inputs, 13 neurons in the hidden layer, and one output. The inputs were the distances between the resonant wavelengths ($\Delta\lambda$) and the attenuation differences (ΔP) in dB between them for each temperature value (ranging from 22°C - 27°C). The hidden activation was a sigmoid function. To improve generalization and provide an uncertainty estimation [26], we added a 10% rate dropout between the hidden and output layers. The output displayed is the estimated CO₂ gas concentration. Databases with 78 samples were generated, and Table III represents a selection of these values for application in the ANN created.

The Nadam algorithm [27] was used to train this network, utilizing 54 samples for training and 12 for validation. The system was evaluated using samples that were not encountered during training to make sure it is dependable. Therefore, 12 samples were utilized to assess the model's performance in order to guarantee a suitable balance between the quantity of data for training and assessment.

TABLE III. PORTION OF DATABASE SAMPLES USED FOR APPLICATION IN ANN.

$\Delta\lambda$ (nm)	ΔP (dB)	CO ₂ (% Concentration)
107.2441	6.37418	0
107.2263	6.37039	10
107.2205	6.36919	20
107.2192	6.36876	30
107.2159	6.36833	40
107.2144	6.3679	50
107.9992	6.28638	0
107.9827	6.28277	10
107.9778	6.28147	20
107.9766	6.28104	30
107.9733	6.28071	40
107.972	6.28028	50
108.764	6.20043	0

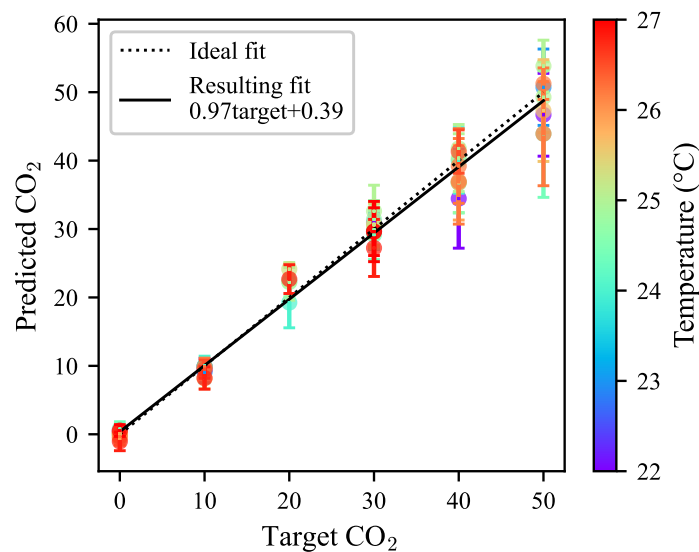


Fig. 7. Results obtained by the ANN training.

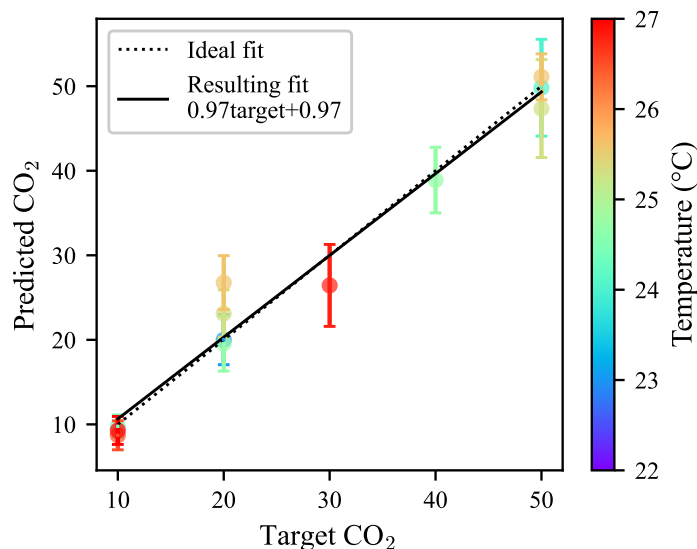


Fig. 8. Results obtained by the ANN validation.

Fig. 7, Fig. 8, and Fig. 9 illustrate the results obtained by the ANN training, validation, and gas concentration tests, with a comparison between the ideal output and the obtained output, which demonstrate the usefulness of the network. Note that uncertainty was estimated using the 10% rate dropout in 20 iterations per measurement.

For the CO₂ gas concentration tests, a mean square error of 4.287 was obtained. Furthermore, a correlation coefficient between the expected output and the output obtained by the network of 0.9928 was found, and a determination coefficient of 0.984. The network is able to correlate all parameters and directly find the concentration of CO₂ without the need to use separate systems for each temperature range. Indeed, we can see in Fig. 9 that the ANN outputs are closely related to the expected output

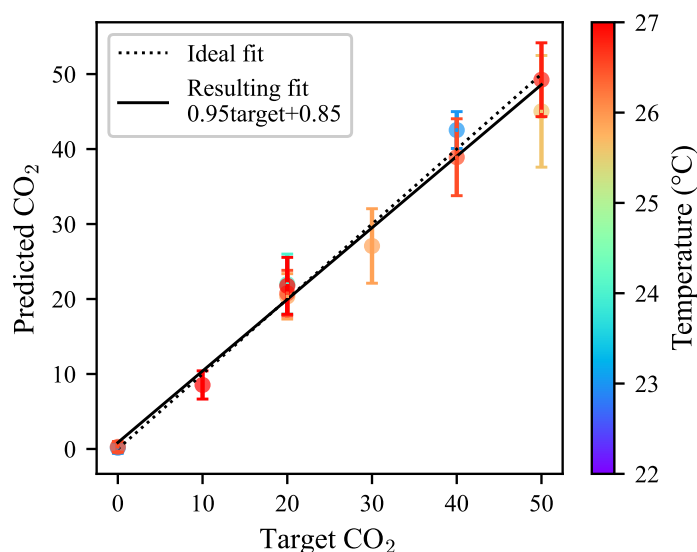


Fig. 9. Results of the gas concentration test obtained by the ANN.

(targets), thus following the identity line that represents an ideal estimator.

IV. CONCLUSIONS

In this work, the development of a refractive index sensing methodology for measuring carbon dioxide concentrations was proposed. In this sense, measurements of the external refractive index were carried out separately, and measurements of its variation were carried out together with temperature, both as a function of the resonance wavelengths of a tapered LPG. To identify the presence of the gas, it is necessary to cover the tapered LPG sensor with a layer sensitive to CO₂.

Through the simulations, it was proven that variations in the temperature of the external environment influence the resonance wavelengths of the LPG when it is sensitive to variations in gases such as CO₂, i.e., the wavelengths resulting from the analysis of the variation of refractive indices external to the fiber also undergo temperature changes.

It is feasible to identify fluctuations in the concentration of CO₂ with a minimal error using the differences in power and spacing between the resonance wavelengths applied to an ANN, demonstrating the usefulness of the network.

Although the focus of this work has been to measure the concentration of CO₂ in the environment and to analyze the influence of temperature (choosing a temperature range of 22°C - 27°C) in the measurement of the refractive index, all the results obtained serve to generate the foundation and knowledge for future research that can be carried out with a wider temperature range or with concentrations of different substances.

ACKNOWLEDGMENTS

Authors would like to thank the financial support from the Conselho Nacional de Desenvolvimento Científico e Tecnológico-CNPq, Coordenação de Aperfeiçoamento de Pessoal de Nível Superior-CAPES, FAPEMIG and Inerge-UFJF.

REFERENCES

- [1] J. Wang, Z. Wen, B. Yang, and X. Yang, "Optical carbon dioxide sensor based on fluorescent capillary array," *Results in Physics*, vol. 7, pp. 323–326, 2017.
- [2] H. Ahmad, M. T. Rahman, S. N. A. Sakeh, M. Z. A. Razak, and M. Z. Zulkifli, "Humidity sensor based on microfiber resonator with reduced graphene oxide," *Optik*, vol. 127, pp. 3158–3161, 2016.
- [3] G. Rego, "A review of refractometric sensors based on long period fibre gratings," *The Scientific World Journal*, vol. 2013, pp. 1–14, 2013.
- [4] F. Esposito, A. Srivastava, L. Sansone, M. Giordano, S. Campopiano, and A. Iadicicco, "Label-free biosensors based on long period fiber gratings: a review," *IEEE Sensors Journal*, vol. 21, pp. 12 692–12 705, 2020.
- [5] Z. Gu, X. Jiang, and H. Chen, "High-sensitivity sensor design based on cascaded long-period fiber grating with film coating," *Optical Engineering*, vol. 53, pp. 021 104–021 104, 2014.
- [6] F. Delgado and A. Bessa, "Comparative study of coupling to symmetric and antisymmetric cladding modes in long-period fiber gratings," *Journal of Modern Optics*, vol. 66, pp. 1369–1374, 2019.
- [7] M. Smietana, W. J. Bock, P. Mikulic, and J. Chen, "Increasing sensitivity of arc-induced long-period gratings—pushing the fabrication technique toward its limits," *Measurement Science and Technology*, vol. 22, pp. 1–6, 2010.
- [8] V. Bhatia and A. M. Vengsarkar, "Optical fiber long-period grating sensors," *Optics letters*, vol. 21, pp. 692–694, 1996.
- [9] J. Liu, Y. Sun, and X. Fan, "Highly versatile fiber-based optical fabry-pérot gas sensor," *Optics express*, vol. 17, pp. 2731–2738, 2009.
- [10] A. Riahi, M. Vahedi, J. Khalilzadeh, and V. Dastjerdi, "Investigation of the effect of the taper geometry on the sensitivity of tapered-fibre gas sensors," *Journal of Modern Optics*, vol. 67, pp. 1259–1266, 2020.

- [11] G. R. C. Possetti, L. C. Côcco, C. I. Yamamoto, L. V. R. De Arruda, R. Falate, M. Muller, and J. L. Fabris, "Application of a long-period fibre grating-based transducer in the fuel industry," *Measurement Science and Technology*, vol. 20, pp. 1–9, 2009.
- [12] R. Z. V. Costa, G. R. C. Possetti, L. V. R. De Arruda, M. Muller, and J. L. Fabris, "Curvature vector smart sensing with a long-period fibre grating probed by artificial intelligence," *Measurement Science and Technology*, vol. 21, pp. 1–9, 2010.
- [13] J. Sun, C. C. Chan, K. M. Tan, X. Y. Dong, and P. Shum, "Application of an artificial neural network for simultaneous measurement of bending curvature and temperature with long period fiber gratings," *Sensors and Actuators A: Physical*, vol. 137, pp. 262–267, 2007.
- [14] J. Sun, C. C. Chan, X. Y. Dong, and P. Shum, "Application of an artificial neural network for simultaneous measurement of temperature and strain by using a photonic crystal fiber long-period grating," *Measurement Science and Technology*, vol. 18, pp. 2943–2948, 2007.
- [15] F. Barino, F. S. Delgado, M. A. Juca, T. V. N. Coelho, and A. B. dos Santos, "Comparison of regression methods for transverse load sensor based on optical fiber long-period grating," *Measurement*, vol. 146, pp. 728–735, 2019.
- [16] K. Hornik, M. Stinchcombe, and H. White, "Multilayer feedforward networks are universal approximators," *Neural networks*, vol. 2, pp. 359–366, 1989.
- [17] F. O. Barino and A. B. d. Santos, "Lpg interrogator based on fbg array and artificial neural network," *IEEE Sensors Journal*, vol. 20, pp. 14 187–14 194, 2020.
- [18] J. Sun, C. C. Chan, N. Ni, K. M. Tan, X. Y. Dong, and P. Shum, "Application of an artificial neural network for simultaneous measurement of bending curvature and temperature with long period fiber gratings," in *Optical Fiber Sensors*, p. TuE78, 2006.
- [19] J. Sun, C. Chan, K. Tan, X. Dong, and P. Shum, "Application of an artificial neural network for simultaneous measurement of bending curvature and temperature with long period fiber gratings," *Sensors and Actuators A: Physical*, vol. 137, pp. 262–267, 2007.
- [20] J. Hromadka, B. Tokay, R. Correia, S. P. Morgan, and S. Korposh, "Carbon dioxide measurements using long period grating optical fibre sensor coated with metal organic framework hku-1," *Sensors and Actuators B: Chemical*, vol. 255, pp. 2483–2494, 2018.
- [21] R. Turner, D. Eriksson, M. McCourt, J. Kiili, E. Laaksonen, Z. Xu, and I. Guyon, "Bayesian optimization is superior to random search for machine learning hyperparameter tuning: Analysis of the black-box optimization challenge 2020," 2021. [Online]. Available: <https://arxiv.org/abs/2104.10201>
- [22] M. A. Jucá, F. S. Delgado, D. D. Silveira, T. V. N. Coelho, and A. B. dos Santos, "Investigation of carbon dioxide sensitivity in long period gratings," in *12º Congresso Brasileiro de Eletromagnetismo; 17º Simpósio Brasileiro de Microondas e Optoeletrônica e Latin American Workshop on Optical Fiber Sensors*, 2016.
- [23] B. M. Lacquet, P. L. Swart, and G. Ameer, "Long-period grating with sol-gel coating for co2 detection," in *Second European Workshop on Optical Fibre Sensors*, vol. 5502, pp. 287–290, 2004.
- [24] T. Allsop and R. Neal, "A review: Application and implementation of optic fibre sensors for gas detection," *Sensors*, vol. 21, 2021.
- [25] "Why tensorflow is so popular – tensorflow features," 2021. [Online]. Available: <https://www.geeksforgeeks.org/why-tensorflow-is-so-popular-tensorflow-features/>
- [26] M. Abdar, F. Pourpanah, S. Hussain, D. Rezagadegan, L. Liu, M. Ghavamzadeh, P. Fieguth, X. Cao, A. Khosravi, U. R. Acharya, V. Makarenkov, and S. Nahavandi, "A review of uncertainty quantification in deep learning: Techniques, applications and challenges," *Information Fusion*, vol. 76, pp. 243–297, 2021.
- [27] T. Dozat, "Incorporating nesterov momentum into adam," pp. 1–4, 2016. [Online]. Available: https://cs229.stanford.edu/proj2015/054_report.pdf